Particuology 115 (2026) 202–213

Contents lists available at ScienceDirect

Particuology

journal homepage: www.elsevier.com/locate/partic

Dust release from various small-scale belt conveyor setups discharging into a wind tunnel – experimental investigation using different limestone qualities

Marcus Weidemann*, Eberhard Schmidt

Institute of Particle Technology, University of Wuppertal, 42119, Wuppertal, Germany

HIGHLIGHTS

- Different limestone fractions discharged into a wind tunnel from a conveyor belt.
- Coarse material emits dust mainly upon impact on the bulk pile.
- The microscopic mechanism can be described by a literature model, consisting of fine dust-laden coarse particles.
- Fine material emits dust mainly by collision of loose agglomerates while falling.
- The microscopic mechanism can be described by a literature model, which consists of agglomerates breaking upon impact.

GRAPHICAL ABSTRACT

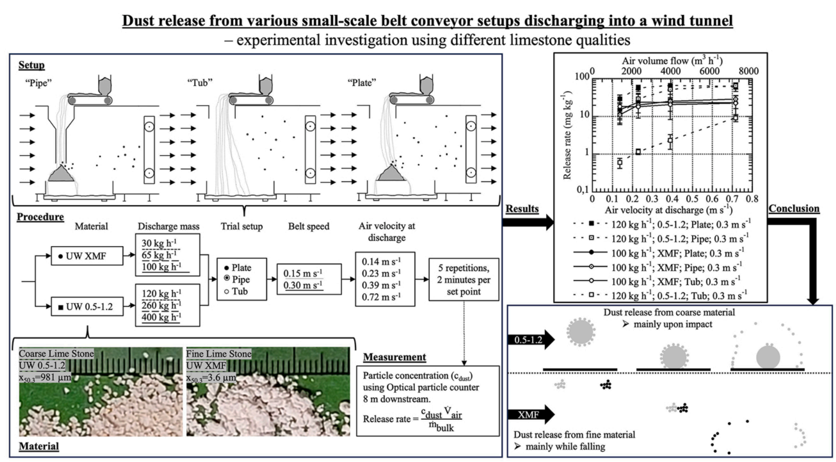

ARTICLE INFO

Keywords:
Dust
Dust release
Bulk material handling
Belt conveyor
Discharge

ABSTRACT

To investigate the release of dust, coarse ($x_{50.3}$ = 980 µm) and fine ($x_{50.3}$ = 3.6 µm) limestone was discharged into a wind tunnel using a model conveyor belt. Different test setups were used to measure the dust release in different phases of the discharge. The discharge mass flow, belt speed and wind tunnel air velocity were varied. Systematic differences were found between the two size fractions. The dust release of the fine material mainly takes place during the fall, while the dust release of the coarse material is dominated by the impact on the bulk pile. For the coarse material, a model for the individual release of dust-laden coarse material particles from the literature can be used as an explanatory approach. A different explanatory approach is required to describe the release of dust from the fine material.

* Corresponding author.
E-mail address: weidemann@uni-wuppertal.de (M. Weidemann).

https://doi.org/10.1016/j.partic.2026.05.016
Received 28 July 2025; Received in revised form 20 April 2026; Accepted 19 May 2026
Available online 28 May 2026

1. Introduction

Airborne particles in the form of dust pose multiple risks. These affect areas such as human health, environmental safety, occupational safety and the longevity of machinery. Managing dust is therefore a goal which is in the self-interest of anyone handling bulk material, and is often obligatory due to laws and regulations. Understanding the origins of dust can help to minimize dust emissions.

Gaining a theoretical understanding of dust generation is a research field with an ongoing debate. Chakravarty et al. (2019) provided an overview of the field summarizing different test methods, release mechanisms, modelling approaches and relevant parameters. Affecting parameters are, among others, particle size and size distribution (Chakravarty et al., 2017; Teipel et al., 2023), moisture content (Londershausen, 2018; Wypych & Mar, 2013), particle density (Saleh et al., 2014), material composition (Saleh et al., 2014), the type of stress put on the material (Bach, 2013), e.g., particle movement by vibration (Kahrizsangi et al., 2015) and fluidization (Saleh et al., 2014).

The dust liberation upon conveyor belt discharge was modeled by Derakhshani et al. (Derakhshani, 2016; Derakhshani et al., 2013) for quartz grains with a mass median of 600 μm. It was shown, that particles can be released during the fall of the bulk and upon impact. Also, the fluid dynamic simulation shows that a turbulent regime with eddies is induced by the fall and impact of bulk material. Roberts et al. (2021) employed a CFD-DEM approach to study the propagation of dust clouds when loading a bulk carrier ship. They concluded that crosswinds and loading behavior can cause dust to exit the ship's cargo hold during loading.

Turkevich et al. (2025) studied a bulk material splash falling onto a plate. A dense dust phase of falling material which is surrounded by a loose dust phase is described. By modeling the movement of the resulting dust cloud expansion over time as well as single particle trajectories, they could show, that the resuspension of particles from the ground by aerodynamic lift forces can be a secondary source of dust. The combination of dense and loose dust phases was also observed by Rheina-Wolbeck (2006) who observed it during the fall of bulk material in a rectangular tube using a camera. He also recognized that the loose dust phase is accompanied by additional airflow and slight pressure changes, which can be manipulated by air extraction. Ansart et al. (2009) studied the combination of a dense phase surrounded by a loose dust phase using particle image velocimetry. They found that the cone of the loose phase widened as the material fell, resulting in additional air being entrapped in the dust phase and particles becoming segregated. Almeida Leão et al. (de Almeida et al., 2020) performed additional modeling of the movement of airborne dust around a falling bulk material stream and identified four zones that contribute differently to dust spreading.

The previous two paragraphs provided an introduction to the macroscopic propagation of dust and dust clouds during bulk material handling. The next two paragraphs present two mechanistic models that offer explanations of dust release on a microscopic scale.

Antonyuk et al. (2006) described a primary dust release mechanism from granular material. By experiment and DEM simulation it was shown, that smaller particles, which can become airborne, can form by shattering of granules upon impact on a surface. The breakage probability of a granule increases with increasing impact speed and that the resulting particle size of the fragments decreases with impact speed. Olaleye et al. (2019) experimentally studied the breakage behavior of tablets, which can be seen as dense agglomerates of the primary powder from which they are pressed. Milling tablets of different porosity showed that the amount of resulting fine material increases with porosity. This finding was confirmed by Weidemann et al. (2023) using inline particle size measurement in dry granulation.

A different microscopic dust release mechanism is suggested by Schulz et al. (2019, 2022) and Woschny et al. (Woschny, 2025; Woschny et al., 2021, 2025). In their model a coarse carrier particle which is coated with fine material is modeled by DEM and experimentally verified. It was shown, that the dust emitted is the fine material which is released upon impact of the coarse particle onto the ground surface or by coarse particle-particle impact. This model limits the maximum dust emission from a single particle to the mass of fine material it carried before the impact. The released dust mass first increases sharply with impact speed, then only increases slightly and, depending on the exact model setup, stagnates at medium impact speed before it further increases sharply at higher impact speeds and then slowly determines to 100 % fine material being released.

The objective of this study is to experimentally investigate the macroscopic dust release during conveyor belt discharge of different limestone qualities. The model approaches from Atonyuk, Schulz and Woschny will be used to explain the macroscopic observations and the differences that results from using different limestone qualities.

2. Material and methods

2.1. Bulk material

Limestone (>99 % $CaCO_3$) Ulmer Weiβ (UW) from Eduard Merkle in the variants UW XMF (XMF) and UW 0.5-1.2 (0.5-1.2) was used as a test bulk material. The particle size distribution by dry dispersed laser diffraction is $x_{90,3} = 5.49$ μm, $x_{50,3} = 3.6$ μm and $x_{10,3} = 1.94$ μm for XMF and $x_{90,3} = 1470$ μm, $x_{50,3} = 981$ μm and $x_{10,3} = 648$ μm with 1.35 %wt being in a secondary mode at $x_{modal} = 2.6$ μm for 0.5-1.2. Conditioned for 24 h at 25 °C and 30 %rH, 50 %rH, 70 %rH, the DustView dust release number, as a measure of dustiness, is 19.3, 24.1 and 21.2 respectively for 0.5-1.2 and 14.4, 13.4 and 11.3 for XMF.

2.2. Experimental setup

A wind tunnel with a length of 23 m is used (see Fig. 1). The square cross-section has an edge length of between 1 m at the inlet and at the measuring point and 1.7 m at the discharge point. The entire tunnel is made of sheet metal and is grounded.

The tunnel consists of five segments (see Fig. 2). The inlet, including the transition piece, is 2.5 m long. The second segment contains the discharge point (as well as four spray nozzles which are not used for this study). It is 8.2 m long including the transition. The third segment contains nine dust probe collection covers. The fourth segment consists of a lamella separator to remove droplets and larger particles. The fifth segment consists of an extraction unit, including a filter for safe particle separation.

A Grimm 1.109 optical particle counter (OPC) with isokinetic sampling is used at the measuring point. The measuring point is located in the center of the 1 m × 1 m square sampling cross-section, 8.5 m downstream from the belt discharge point. This position was chosen in order to measure dust emissions that can be transported over long distances and are environmentally relevant. A conveyor belt (length 140 cm, width 11.5 cm, speed 0.01 to 0.3 m s^{-1}) is positioned on top of the tunnel at the belt discharge point. Its end is positioned over a rectangular long hole in the tunnel ceiling. The parts of the hole that are not needed are closed with sheet metal covers. The conveyor belt is fed with a constantly adjustable bulk material mass flow by a Brabender DDW-M-FW80 screw feeder. A tub with overflow protection is positioned under the wind tunnel. It can be moved with a pallet truck. The tub can be filled with water. In addition, a water nozzle is installed, to flush away any bulk cones in the water before they form. If not used the tub is covered with sheet metal covers.

Depending on the type of stress investigated, different setups are used to release dust in the tunnel. These are shown in Fig. 3. To measure the dust release from a bulk material at rest ("Bulk"), a bulk cone is placed on a plate with a diameter of 20 cm on a 13 cm high table in the

Fig. 1. Overview of the wind tunnel test facility.

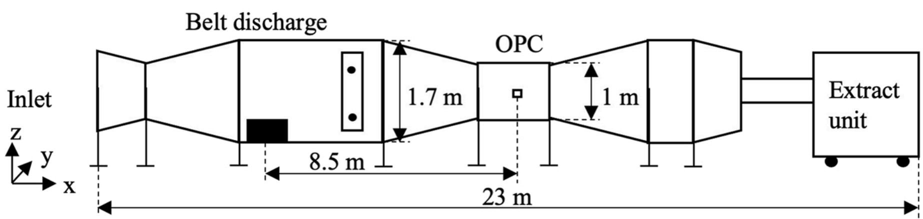

Fig. 2. Schematic view of the wind tunnel.

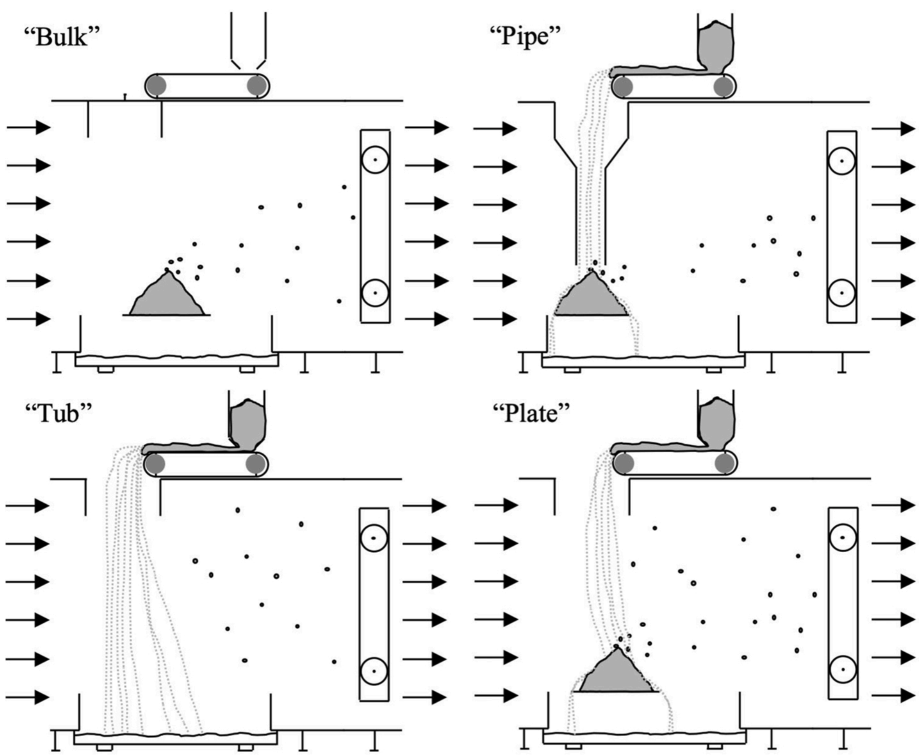

Fig. 3. Variations of the test setups at the belt discharge point (screw feeder for filling the conveyor belt not shown).

tub. To measure the dust release during the belt discharge of bulk material, material is continuously dropped onto the plate using the conveyor belt ("Plate"). This way a constant bulk cone is produced. Excess material falls into the water tub, ensuring a constant pile height and constant resulting drop height. A pipe with a diameter of 140 mm is installed between the tunnel roof and the bulk cone in order to isolate the dust release upon impact ("Pipe"). In order to isolate the dust release during the free fall ("Tub"), the material is dropped directly into the water tub.

2.3. Experimental method

The mean flow velocity at the discharge point is set to 0.72, 0.39, 0.23 or 0.14 m s^{-1}. The resulting mean velocities at the measuring section and the corresponding air volume flows are listed in Table 1. The flow velocity at the discharge point (v_{Air}) is varied by setting a manual throttle valve (positioned between lamella separator and extract unit) and the frequency inverter of the extract unit to predefined values.

Within a single measuring run, the discharge mass flow and flow

Table 1
Set flow velocity at OPC measuring point with corresponding mean flow velocity at discharge point and the resulting volume flow rate.

OPC	Discharge	Volume flow
2.10 m s^{-1}	0.72 m s^{-1}	7320 m^3 h^{-1}
1.14 m s^{-1}	0.39 m s^{-1}	3973 m^3 h^{-1}
0.67 m s^{-1}	0.23 m s^{-1}	2335 m^3 h^{-1}

velocity are varied according to the test matrix given in Table 2. For each test setting, the dust number concentration per size class is measured for 2 min, mean values are taken every 6 s. The measurement order in each run is randomly determined, only the measurement point “0.39 m s^{-1}, medium” is always used as an anchor point and carried out as the first and last measurement as well as after the first and second third of the measuring run. The discharge quantity ($\dot{m}_{UW}$) is set on the screw feeder via a PID controller. Due to the different bulk material flow properties of the two materials, different mass flow settings had to be selected.

The test matrix is repeated five times for each parameter set. The material, the test setups for the respective type of stress and conveyor belt speed is varied as shown in Fig. 4. The “Bulk” setup variant is not taken into account because the amount of dust released cannot be detected within the scope of the measurement accuracy.

2.4. Data preparation

From the number concentrations per particle size class recorded with the Grimm 1.109 optical particle counter, number-related distribution sums and distribution densities were calculated. The number-related distribution was converted into the volume-related distribution using the moment method (Schmidt, 2001). The upper decile, lower decile and median were calculated for both cases by linear interpolation from the distribution sum. To determine the dust mass concentration from the number concentration, ideal spheres with the diameter of the respective measurement interval center and the solid density of limestone (2680 kg m^{-3} (Londershausen, 2018)) were assumed. The total dust concentration in μg m^{-3} was calculated by summing. The resulting calculated total dust concentration is consistently 19 % higher than the total dust concentration calculated by the Grimm 1.109 default setting. This difference can be attributed to the density of limestone being used for the calculation instead of a density for an unspecified typical particle, which is assumed by the optical particle counter.

The dust load was determined by multiplying the total dust concentration by the set air volume flow. The set air volume flow is the product of the set flow velocity at the measuring point and the cross-sectional area of 0.968 m^2.

The release rate relates the measured dust load to the discharged bulk mass in the corresponding time period. The retention time shift between the OPC measuring point and the discharge point due to the retention time in the tunnel section was taken into account for the specific flow.

For dust concentration, dust load, release rate and mass median size the mean values of the fivefold measurement were given, including the single standard deviation.

2.5. Statistical analysis

To estimate statistical significance, a multivariate regression analysis was carried out using the Excel Data Analysis add-on. To include the non-numerical variables of the trial setup, numerical values were assigned to them: plate 0, pipe 1, and tub 2. Individual variables with p-values >0.05 are deemed insignificant; those with p-values <0.05 are significant; those with p-values <0.01 are very significant; and those with p-values <0.001 are highly significant.

3. Results and discussion

3.1. Preliminary consideration of the particle movement in wind tunnel

For the calculation of the particle trajectory, a drop height of 1.7 m (channel height) was assumed, with a constant horizontal flow velocity of 0.4 m s^{-1} (corresponding to 1.2 m s^{-1} at the measurement point) and no eddy formation. Taking into account gravity, inertia, lift and flow resistance, and assuming laminar flow, the position of a particle over time can be determined using equations (1) and (2), Using the particle diameter d, the particle bulk density ρ_p(UW, XMF) = 2680 kg m^{-3}, the gravitational acceleration g, time t, and the viscosity η_{Air}(20 °C, 1 bar) = 1.821 × 10^{-5} Pa s (VDI-Gesellschaft et al., 2013).

$$z_P(t) = h_{Tunnel} - \frac{d^2\,\rho_p}{18\,\eta}\,g\left[t + \frac{d^2\,\rho_p}{18\,\eta}\left(e^{-\frac{18\,\eta}{d^2\,\rho_p}t} - 1\right)\right] \tag{1}$$

$$x_p(t) = v_{Air}\left[t + \frac{d_p^2\,\rho_p}{9\,\eta}\left(e^{-\frac{9\,\eta}{d_p^2\,\rho_p}t} - 1\right)\right] \tag{2}$$

Particles of different sizes thus follow different trajectories, as shown in Fig. 5. At a distance of 8.5 m from the release point, particles smaller

Table 2
Text matrix for a single measuring run.

$\dot{m}_{UW}$	v_{Air} = 0.14 m s^{-1} (1394 m^3 h^{-1})	v_{Air} = 0.23 m s^{-1} (2335 m^3 h^{-1})	v_{Air} = 0.39 m s^{-1} (3973 m^3 h^{-1})	v_{Air} = 0.72 m s^{-1} (7320 m^3 h^{-1})
Low	2 min	2 min	2 min	2 min
Medium	2 min	2 min	4 × 2 min	2 min
High	2 min	2 min	2 min	2 min

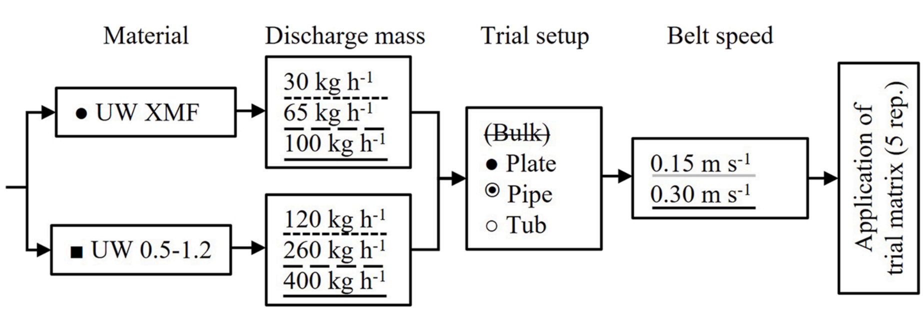

Fig. 4. Overview of the performed test program.

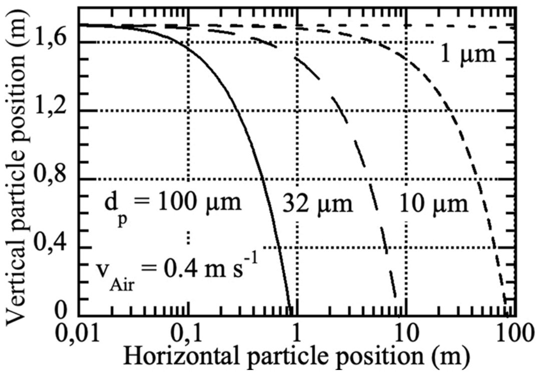

Fig. 5. Calculated particle trajectory for particles of different sizes, starting from the release point.

than 10 μm reach the measuring point almost entirely, while particles larger than 32 μm settle and deposit in the wind tunnel.

3.2. Bulk setup dust emissions

Due to the low dust emission from the "Bulk" setup, the dust release cannot be distinguished from the background concentration for either material. This is likely because the air velocities at the discharge point are too low, ranging from 0.14 to 0.72 m s^{-1}, to generate enough lift forces to detach dust particles from the bulk.

3.3. Dust emission from belt discharge for XMF

The results for XMF are presented by first demonstrating the connection between dust concentration, dust load and release rate. The influences of the individual test parameters on the dusting are then discussed using the release rate. Finally, the particle size is addressed.

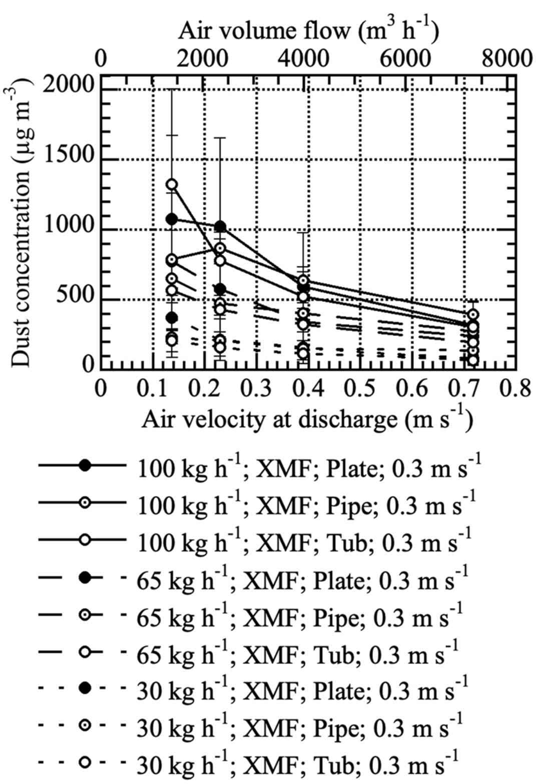

Fig. 6. Measured dust concentration as a function of air velocity for different stress types and discharge mass flows for XMF.

Fig. 6 shows the measured dust concentration during the conveyor belt discharge of XMF as a function of the air velocity ($p = 3.0 \times 10^{-14}$). The graphs for the discharge quantities 100, 65 and 30 kg h^{-1} are shown for the drop including impact ("Plate"), the drop isolated from air current ("Pipe") and for the in-current drop without impact ("Tub") at a belt speed of 0.3 m s^{-1}. It can be seen that the dust concentrations sort by discharge rate ($p = 4.0 \times 10^{-23}$), high dust concentration with high discharge rate, low concentration with low discharge rate. Yet the measured values show a high standard deviation. On the one hand, this can be explained by the turbulent flow. In order to reach the inlet of the isokinetic sampling, the particles released at a specific location must move with the streamline that reaches the inlet of the isokinetic sample inlet. Thereby, a measurement variance caused by the turbulent flow occurs during transmission from the point of emission to the sampling point. In addition, the dust can be emitted both in free fall and upon impact with bulk pile. This emission-related variance is, for small particles moving with the flow, resolved by the turbulent mixing in the further wind tunnel. Furthermore, it can be seen that the dust concentration is qualitatively similar regardless of the type of stress ($p = 0.18$).

It is noticeable that the overall dust concentration decreases with the flow velocity. This can be explained by a dilution effect with increasing air volume flow. If the dust load is considered, this dilution effect can be eliminated. Fig. 7 shows the dust load as a function of the flow velocity for the discharge of XMF onto the plate at different air currents. It can be seen that the dilution effect disappears completely. Within the measurement uncertainty, the dust load for the in-current drop including impact is independent of the air velocity ($p = 0.14$). It can still be seen that the dust load increase with the discharge rate is highly significant ($p = 1.9 \times 10^{-7}$).

In the next step, the dust load is related to the discharge quantity in order to determine the release rate as a principally dimensionless emission measure. The release rate is represented as dust mass in mg per kg of bulk material discharged.

Fig. 8 shows the release rate as a function of the air velocity for the three stress types at a constant discharge rate of 65 kg h^{-1}. It can be seen that the release rate increases with air velocity. Although this increase is within the measurement variance and therefore cannot be definitively verified ($p = 0.10$). Overall, the release rates are at a similar level regardless of the stress type and increase slightly linearly with the flow ($p = 1.9 \times 10^{-5}$), whereby the graphs partially cross each other. The finding that the dust release is largely independent of the stress type is

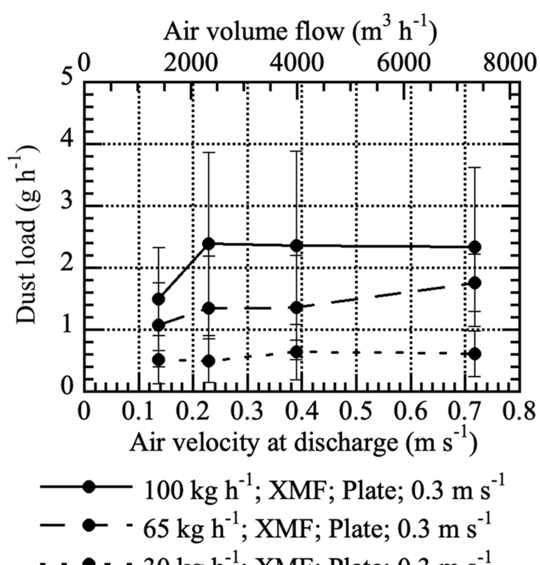

Fig. 7. Total dust load as a function of air velocity for different discharge rates for in-current drop onto the bulk pile "Plate" for XMF.

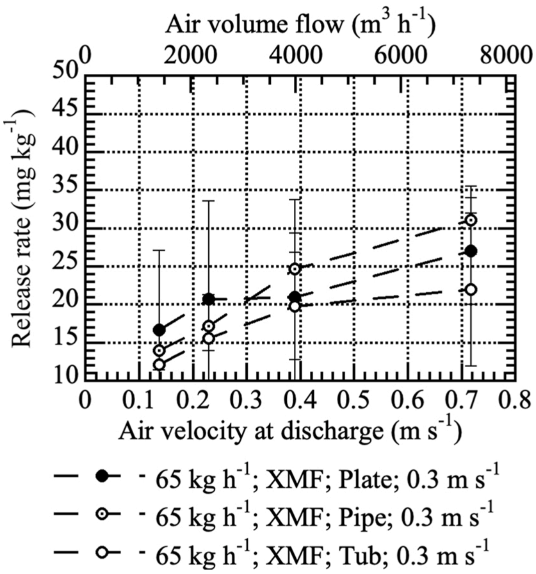

Fig. 8. Influence of stress type on release rate for XMF.

remarkable. The test setup should isolate the different release mechanisms in free fall and upon impact. When dropping into the water tub, dust emissions due to impact on the bulk pile can be reliably prevented, particularly as the surface tension of the water was diminished by adding detergent to prevent particles from bouncing off the water surface. Although the horizontal air flow can be prevented when discharging through the 140 mm diameter pipe it could not be prevented, that air is being sucked through the pipe resulting in a vertical in pipe air flow. Complementary flow measurement in the pipe showed that the total air velocity cannot be reduced. The only difference is that the main flow direction changes from horizontal in the wind tunnel to vertical in the pipe. Therefore, interaction between the loose XMF agglomerates during the fall cannot be prevented or reduced by the pipe.

The relative indifference among the three stress types indicates that the primary source of particle emissions must be common to all stress types. This suggests that the dust release for the fine-grained XMF is dominated by a release mechanism during the fall and that the dust release on impact plays no or only a minor role.

As "pipe" is the only stress type for which there is a steady upward trend, Fig. 9 shows the release rate for all discharge quantities at a constant belt speed of 0.3 m s^{-1}. It can be seen that the release rate increases highly significantly ($p = 1.9 \times 10^{-15}$) with increasing air velocity. But the differences between the release rates are within the measurement variance. This may be due to the fact that as the tunnel flow increases, the air flow drawn through the pipe also increases. This can lead to greater dispersion of the agglomerates within the pipe. Though the standard deviation increases significantly, especially at higher flow velocities. It is therefore not possible to conclusively assess whether the upward trend will continue or whether it will begin to stagnate, similar to the stress types “Tub” and “Plate”. Looking at the graphs for 65 and 100 kg h^{-1} individually, the increase flattens out at flow velocities above 0.4 m s^{-1}. Only the 30 kg h^{-1} graph shows a constant increase, whereby the value at 0.72 m s^{-1} shows a high standard deviation, which can be explained by a single high measurement outlier.

In addition, the influence of the belts discharge velocity was investigated. This is shown in Fig. 10. All test settings were carried out at 0.15 and 0.3 m s^{-1} belt speed, see Fig. 4. Over all test settings and experiments the trends at 0.15 m s^{-1} are qualitatively the same as those at 0.3 m s^{-1}. But the overall release rate is slightly lower. In most cases no completely clean trend was measured, in which all release rates at 0.15 m s^{-1} are lower than those at 0.3 m s^{-1}. This is due to the small difference compared to the measurement variance. For the stress type “Pipe”, a consistently lower release rate is shown at 100 kg h^{-1}. Looking at the error indicators (single standard deviation from fivefold measurement), it can even be seen for this selected sample that the differences due to the release rate are comparatively small, resulting in a p-value of 0.10. The slight increase of the release rate with discharge velocity indicates a minor additional dispersion of the XMF agglomerates due to an increased entry velocity into the ambient air.

Using a laser diffractor with compressed air dispersion, a mass median of 3.6 μm was measured for the bulk material XMF. The airborne particles released during bulk material discharge, measured with the OPC, have an almost identical particle size distribution as the bulk XMF. Fig. 11 shows the measured mass median of the dust over the flow velocity for the three stress types. It can be seen that the dust particle size during the discharge of XMF is independent of stress type and flow velocity. The discharge quantity and velocity also have no influence. This shows that the proportion of the bulk material that passes into the air as dust and remains there is not present as an agglomerate but is fully dispersed particles. A possible mechanism of dispersion is discussed further below. Larger XMF agglomerates that detach from the dropping

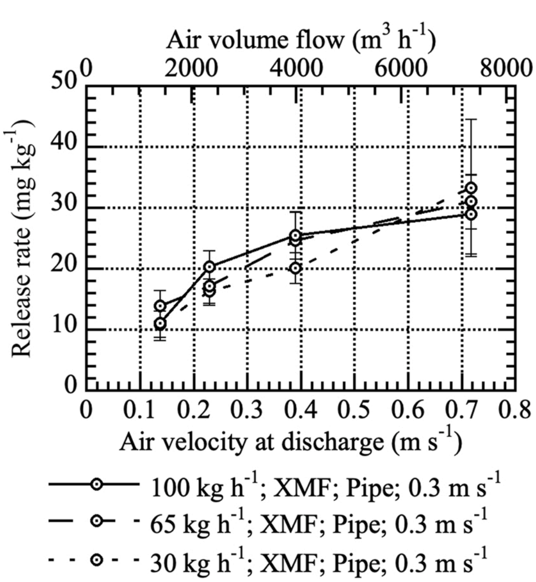

Fig. 9. Influence of the discharge quantity on the release rate for XMF.

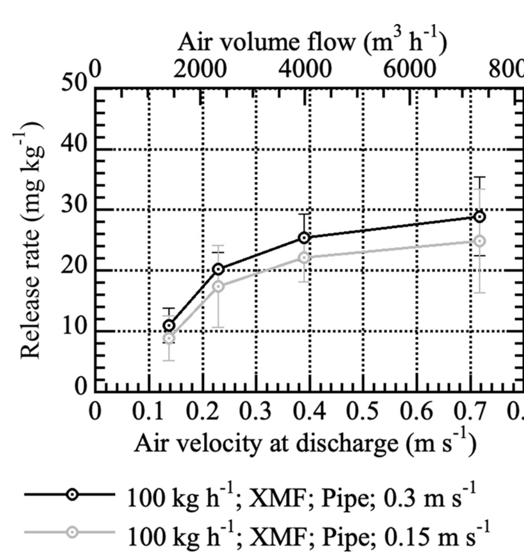

Fig. 10. Influence of belt discharge speed (0.3 and 0.15 m s^{-1}) on the release rate for XMF.

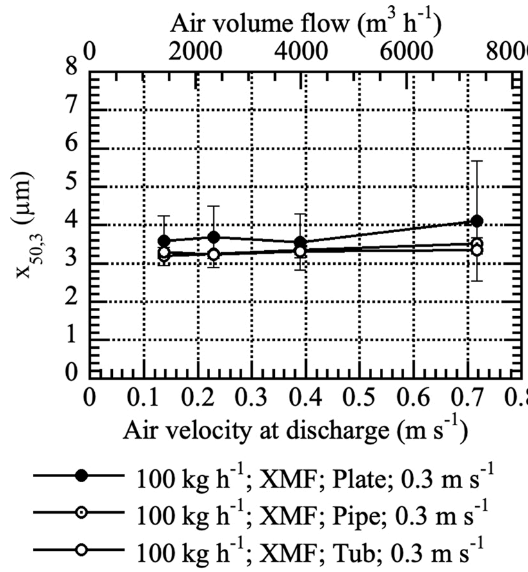

Fig. 11. Influence of the type of stress on the particle size of airborne dust for XMF.

bulk material strand and which are not completely dispersed sink to the ground close to the pile due to their larger diameter.

3.4. *Dust emission from belt discharge for 0.5-1.2*

The dusting behavior of the Ulmer Weiβ 0.5-1.2 bulk material is illustrated using the release rate. Fig. 12 shows the release rate of 0.5-1.2 as a function of the air velocity at a belt discharge speed of 0.3 m s^{-1} for

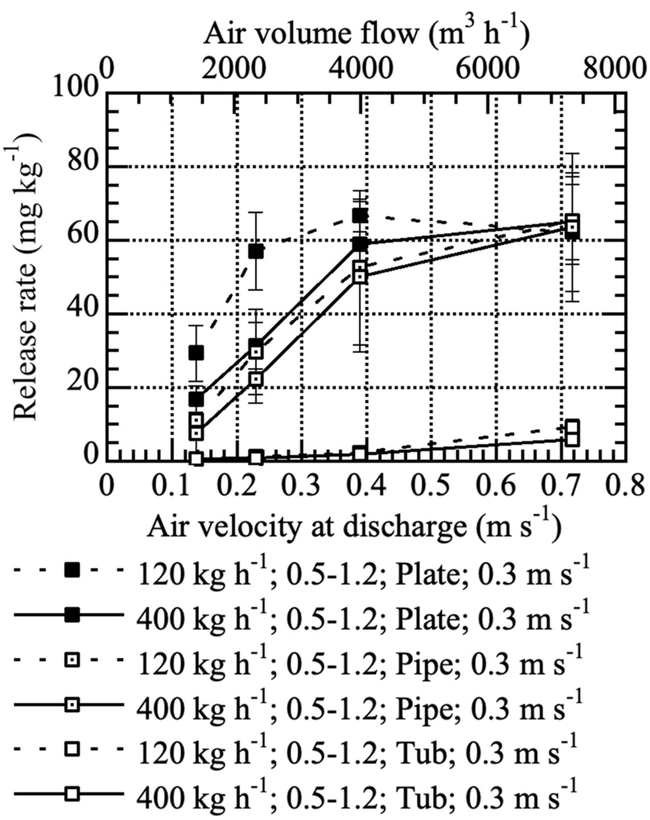

Fig. 12. Influence of discharge quantity and stress type on the release rate for 0.5-1.2.

all stress types at low (120 kg h^{-1}) and high (400 kg h^{-1}) discharge mass flow.

A comparison of the stress types shows clear qualitative and quantitative differences. If the impact on the bulk pile ("Plate", "Pipe") is taken into account, the release rate is significantly higher than without impact ("Tub"). This shows that for the coarser bulk material, the release of dust due to the impact on the bulk pile plays a dominant role compared to the release during free fall. But the dynamics of the release rate with the flow velocity are clearly different with and without impact. With impact, the release rate rises sharply in the range from 0.14 to 0.39 m s^{-1}; with a further increase in flow velocity, the release rate increases only slightly. In the case of in-current drop with impact ("Plate") for 120 kg h^{-1}, it decreases slightly, whereby stagnation within the measurement variance can also be assumed here. It is noticeable that the release converges to the same value for the "Pipe" and "Plate" cases regardless of the mass flow. This suggests that a plateau has been reached. For the inflow drop without impact ("Tub"), there is an exponential increase in the release rate with the flow velocity. This can be seen more clearly in Fig. 15 due to the logarithmic scaling of the axes. Extrapolation of the exponential curve without impact, whilst assuming further stagnation for the stress types with impact, indicates that the release with and without impact are at the same level from a flow velocity of around 1.33 m s^{-1} at the discharge point. Furthermore, it can be seen that a low discharge mass flow rate favors a high dust release, regardless of the type of stress. Only for the flow velocity of 0.72 m s^{-1} does the effect of the discharge mass flow disappear for the load types with impact.

The influence of the discharge velocity is shown in Fig. 13. For the stress types with impact, the release rate decreases with decreasing discharge velocity. In contrast, the release rate without impact ("Tub") is higher at a discharge velocity of 0.15 m s^{-1} than at 0.3 m s^{-1}. This further indicates that the mechanism of dust release in free fall differs from that of impact on the bulk material. It is noticeable that the value to which the release rate determines also decreases with decreasing discharge velocity. This behavior also occurs for the values not shown at 0.3 m s^{-1} for 120 and 400 kg h^{-1}.

The resulting dust particle size is shown in Fig. 14. No influence of the air velocity can be seen for the cases "Plate" and "Pipe". The median mass-based particle size is 3.6 µm and 3.8 µm respectively, which

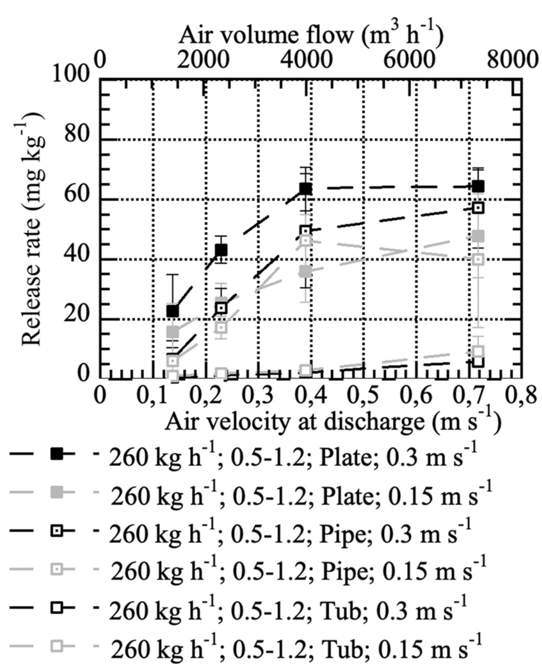

Fig. 13. Influence of belt speed on the release rate for 0.5-1.2.

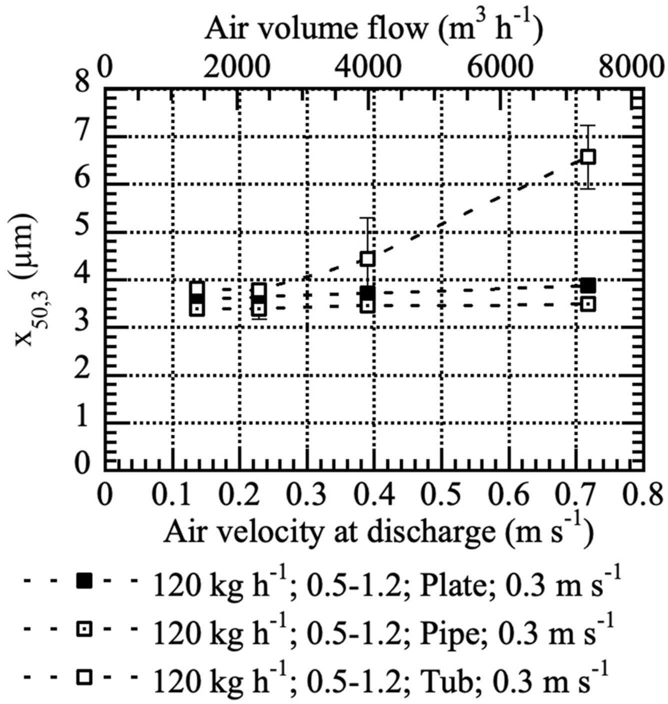

Fig. 14. Influence of stress type and air velocity on the particle size of airborne dust for 0.5-1.2.

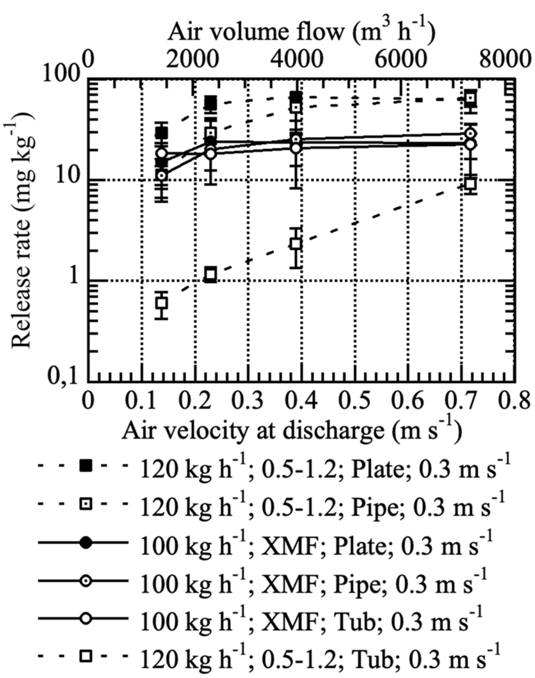

Fig. 15. Influence of air velocity on release rate for different materials and stress types.

corresponds to the fine mode in the particle size distribution of the 0.5-1.2 bulk material. This suggests that the released dust is the fine fraction of the bulk material. For the case without impact (“Tub”), the average dust particle size increases significantly for air flows larger 0.4 m s^{-1}. Assuming that this is also material from the fine fraction of the bulk material, there are two possible explanations for this. On the one hand, it is possible that the release of dust during free fall primarily releases larger particles or agglomerates from the bulk material. Another possible explanation is the influence of sedimentation in the wind tunnel. The calculated sedimentation height of a 10 μm particle between the discharge and sampling point for the given wind tunnel setting at 0.4 m s^{-1} is around 10 cm. With a channel height of 1.7 m, the influence of sedimentation can therefore be estimated to be low. This strengthens the assumption of a selective detachment of coarser particles or agglomerates from the falling bulk material.

3.5. Bulk material comparison

A direct comparison of the two chemically identical limestones Ulmer Weiβ XMF and Ulmer Weiβ 0.5-1.2 allows conclusions about the influence of the particle size of a bulk material on the dusting behavior. The release rate is particularly suitable for this, as it normalizes the influence of the discharge quantity. In order to further reduce the influence of side effect, the highest release rate of 100 kg h^{-1} for XMF and the lowest release rate of 120 kg h^{-1} for 0.5-1.2 are compared in Fig. 15. Furthermore, a logarithmic scaling was selected in order to be able to represent the dynamics of the increase in XMF for the “Tub”. The result shows a significant deviation between the two materials. For 0.5-1.2, the clear difference between the load types with impact on the bulk pile (“Plate”, “Pipe”) and the load type without impact (“Tub”) shows that the dust release for the coarse material is mainly dominated by the dust release upon impact. Here an exponentially increasing dust release can be seen for “Tub”, whereby the dominance of the impact could potentially disappear for higher airflow velocities. For XMF, it can be seen that the differences between the stress types are significantly smaller, which shows that the release mainly takes place during the fall. The influence of the air velocity is also significantly lower for XMF. The release rate is constant for the stress types “Plate” and “Tub”. An increase is not clearly detectable due to the measurement variance. An increase is only visible when falling through the pipe. For 0.5-1.2, an initial increase followed by stagnation can be seen for “Plate” and “Pipe”, although this effect is much more pronounced for the case protected by the pipe.

3.6. Comparison to literature models

The qualitatively and quantitatively different behavior of the coarse and fine limestone suggest different dust release mechanisms. For 0.5-1.2, a model by Schulz et al. for determining dust release (Schulz et al., 2022) can be used as an explanatory approach. A separate explanation model is developed for XMF, as the model mentioned does not provide a satisfactory explanation.

Schulz et al. (2022) analyze dust detachment upon impact of a single coarse particle covered in fine material, shown here schematically in Fig. 16. With the help of a DEM model, a prediction function of the dispersion rate is calculated. It is further validated by experimental data. The dispersion rate describes the ratio of the released fine particles to the fine particles adhering to the coarse material particle before the impact. A coarse particle loaded with fine material corresponds to a bi-modal particle size distribution, with a fine and a coarse mode, which makes the Schulz model a close approximation a single 0.5-1.2 particle, see also Fig. 18.

Fig. 17 left (Schulz et al., 2022) shows the change in the dispersion rate over the impact velocity on different plate materials. In addition to the DEM model, the results of a simplified model function are also shown. Initially, the dust release increases rapidly with increasing impact velocity, whereby this increase is significantly steeper for the impact on the harder metal plate compared to the POM plate. As the impact speed increases further, an intermediate plateau is reached, at which point all the fine particles adhering to the southern hemisphere have fallen off. Subsequently, the dust release continues to increase and determines towards 100 %, which corresponds to a dust release from the northern hemisphere.

Fig. 17 right shows that the bulk material 0.5-1.2 releases dust primarily upon impact on the pile. This effect is characterized by a plateau

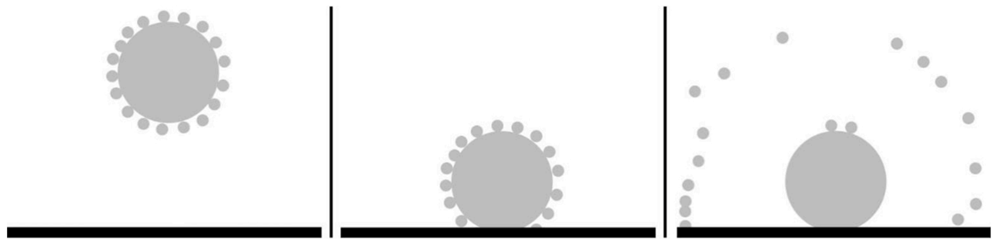

Fig. 16. Scheme of impact for material 0.5-1.2. Dust loaden particles detach fine material upon impact on the floor.

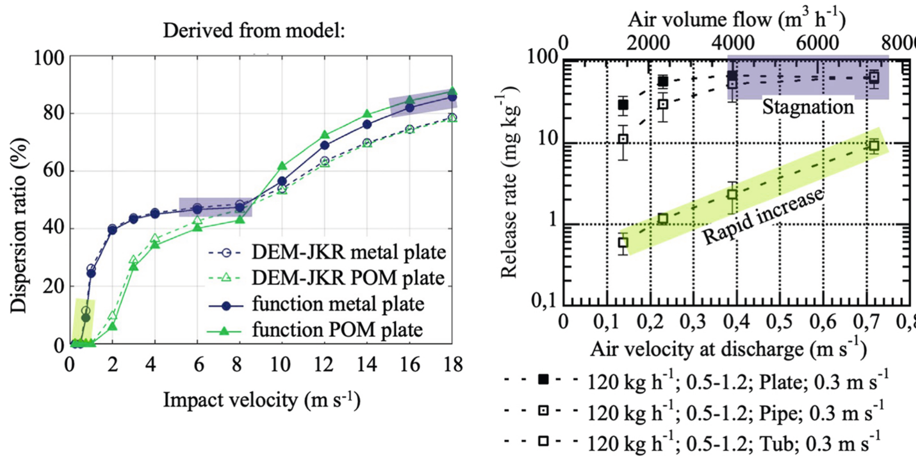

Fig. 17. left: Prediction function for dust release during single particle impact according to Schulz et al. (2022), right: Dust release during belt discharge of 0.5-1.2 bulk material into the wind tunnel.

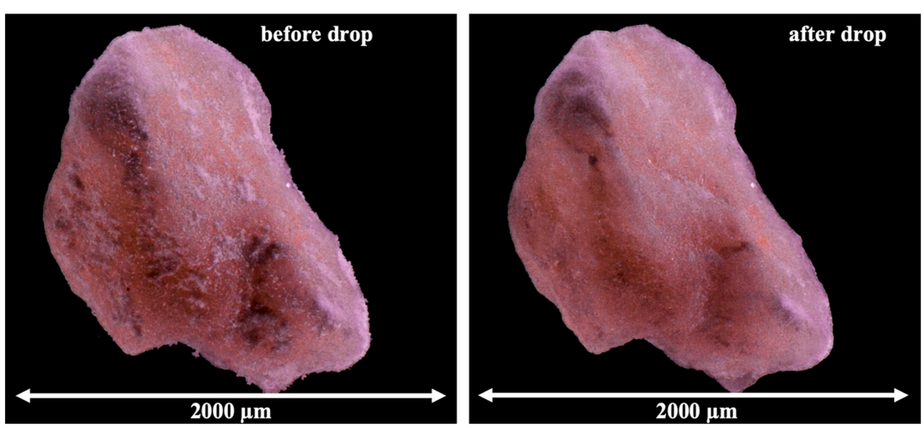

Fig. 18. Microscopy of an Ulmer Weiβ 0.5-1.2 particle with adhering dust before and after individual dropping onto a metal plate from a height of 2 m.

at higher flow velocities. The lower dust release during falling, on the other hand, increases strongly with the flow velocity. The drop height is 1.7 m, a complete conversion of the potential into kinetic energy results in a theoretical impact velocity of 5.77 m s^{-1}, which is plausible as the material falls in a bulk strand. In contrast to the individual particle sedimentation the air friction can be neglected without generating a significant error. The dispersion rate predicted by the model stagnates at 5.77 m s^{-1}. In order to calculate the impact velocity of a single particle, the horizontal air velocity at the drop point must be added using vector addition to the theoretical vertical sinking velocity. This results in impact velocities of 5.78 to 5.81 m s^{-1} depending on the wind tunnel speed. The dispersion rate of a single particle should remain approximately constant in this range. Though the measured release rate for the drop onto the plate increases significantly from 22 to 64 mg kg^{-1}, and stagnation can only be seen in the range of flow velocities higher than 0.4 m s^{-1}. This can be explained by the fact that sedimentation of the dust particles plays a greater role at low flow velocities, which reduces the release rate measured downstream. Due to the near-ground release of dust upon impact with the bulk pile, the sedimentation distance to be covered is shorter for released particles. On the other hand, for particles released during the 1.7 m fall sedimentation is less relevant. In addition to sedimentation, in the case of continuous conveyor belt discharge onto a bulk pile, it should be noted that particles that have already been released can potentially be deposited on the following falling bulk material particles, which means that the release rate should be lower than predicted by the single particle discharge. For the 0.5-1.2 bulk material, there is 1.34 % of the mass in the fine fraction mode which corresponds to 13,400 mg kg^{-1}. A dispersion rate of 50 % would therefore correspond to 6700 mg kg^{-1} and is thus three orders of magnitude higher than the measured values. This shows that additional effects must be taken into account when releasing dust from the bulk material compared to single particle discharge literature model. These include the potential separation of upwardly released fine particles by following falling coarse particles as well as the deposition of downward released fine particles in the bulk pile. Especially due to the separation by following particles, it would follow that the net dust release from the bulk material takes place at the boundary areas between the bulk material phase and the surrounding fluid. In the center of the falling bulk material flow, release and separation potentially balance each other out. One indication in favor of this hypothesis is that a lower belt discharge velocity reduces the release rate. Due to the lower discharge velocity, the bulk material mass flow is expanded less during discharge, the diameter of the falling bulk material strand remains smaller, which reduces its surface area and thus the phase boundary between the bulk material and the fluid phase. As a result, it can be explained why the dust release decreases with decreasing belt speed.

For 0.5-1.2, the case without impact ("Tub") must be considered separately. Here, the dust release can be explained by particle-particle collisions, not by particle-ground collisions. What is striking here is the strong dependence on the flow velocity. The particle-particle collision was also modeled by Saleh et al. (2014). The course of the dispersion rate here is similar to that of the particle-plate collision. Steep increase up to 50 % dispersion rate, intermediate plateau, determines towards 100 %. For particle-particle contact the intermediate plateau extends over a wider impact velocity range. The steep increase in the dispersion rate at low collision velocity in the model explains the steep increase in the release rate with increasing flow velocity. The air flow induces particle-particle collisions. The air flow at the discharge point is in the range 0.1 and 0.7 m s^{-1}. This range is characterized in the model by a steep increase in the dispersion rate, which is reflected in the measured release rate. Fig. 13 shows that, in contrast to the stress types with impact, for the drop without impact ("Tub") the dust increases at a lower belt discharge velocity. This can be explained by more frequent particle-particle collisions in a narrower bulk material strand.

Overall, it was shown that the model developed by Schulz et al. (2022) is suitable for explaining the mechanisms of dust dispersion at the individual particle level for Ulmer Weiβ 0.5-1.2. For a complete description of the dusting behavior during belt discharge of 0.5-1.2 as bulk material, further mechanisms of re-attachment, deposition, sedimentation and transmission must be considered.

The model of Schulz is not applicable for the material XMF due to its fine monodisperse particle size distribution. Here, the measurement results show that the dust release is dominated by the release during the free fall, whereby the release rate increases moderately with the wind

Fig. 19. Microscopy of a loose Ulmer Weiβ XMF agglomerate.

tunnel air flow, but is superimposed by a high measurement variance, which makes detailed statements difficult. The dust release mechanism assumed here is that XMF agglomerates, see Fig. 19, collide with each other in the air and are completely or partially dispersed in the process, see Fig. 20. The approach is more similar to the model proposed by Antonyuk et al. (2006). This is due to the macroscopic structure of the source material which is fine primary particles which tend to agglomerate. If the material would be fully dispersed directly upon belt discharge, a sedimentation distance of about 1 km would be expected due to the fine particle size of $x_{50,3}$ = 3.6 μm, which would result in a release rate of 100 % (10^6 mg kg^{-1}). The measured release rate is in the range of 10 to 40 mg kg^{-1} and thus lower than 0.5-1.2.

The presented model approaches on the microscopic particle release scale can in part explain the measured behavior of the macroscopic release rates. Especially the difference between the fine XMF and the coarse 0.5-1.2 can be explained by the discussed models. Measured release rates were shown to be multiple orders of magnitude lower than predicted by microscopic release mechanisms alone. This requires a discussion of the potential effects causing this.

Firstly, the particles or respective agglomerates released from the bulk on a microscopic scale have a particle size distribution that is influenced by the kinetics of the impact. For fine materials that fall in agglomerated structures, such as XMF, the particle size of the detachments decreases with impact velocity, compare Fig. 21. With increasing impact velocity, the resulting fractures reduce in size, while the agglomerates eventually stay intact at low impact velocities. Additionaly, for fine particles adhering to larger particles, such as 0.5-1.2, Schulz et al. (2022), described the effect of saltation, where individual particles of the fines fraction collide and agglomerate with other particles of the fines fraction during the process of detachment from the large carrier particle. Therefore, for both material types, mechanisms are present that increase the size of the detaching particle agglomerates.

Secondly, most of the bulk material falls in a dense phase (Derakhshani, 2016; Rheina-Wolbeck, 2006; Turkevich et al., 2025). The microscopic particle detachment must therefore be seen in this context. While falling, small particles detaching from an agglomerate or larger particle will be in close proximity to the next agglomerate or large particle, to which they may be reattached or re-agglomerated. When falling on the ground, or more likely onto the bulk pile, a large fraction of the detached particles will be released downwards onto the pile and settle there instead of being emitted into the surrounding air. The fraction that is released upwards is likely to interact, therefore reattach or re-agglomerate, with the following falling bulk material. Therefore, only a small part of the dust that was at some point microscopically detached from the agglomerate or carrier particle will eventually leave the dense phase.

Thirdly, the loose dust phase surrounding the falling dense phase (Derakhshani, 2016; Rheina-Wolbeck, 2006; Turkevich et al., 2025) is influenced by the dense phase (de Almeida et al., 2020; Derakhshani, 2016), inducing an air flow. The looser phase can include eddies and follows the falling dense bulk phase, falling towards the ground. The resulting dust cloud is therefore likely to move towards the ground and be spread in the proximity of the area where the falling bulk material hits the bulk pile. These literature model predictions are backed by visual observations of dust cloud movement during the experiments.

Fourthly, sedimentation will reduce the amount of dust reaching the sampling point. This is especially true for particles or agglomerates larger than approximately 10 μm. As discussed above, the material detaching on a microscopic level is likely to consist of a mixture of primary particles and agglomerates. The agglomerates are likely to be susceptible to sedimentation, which can be confirmed by the observation of limestone sedimentations, which were not quantified, being present in the wind tunnel after the trials.

Taking into account these four points, the material reaching the sampling point, reflects the part of the macroscopic dust emissions that are small enough to stay airborne for a long time. Thus making this

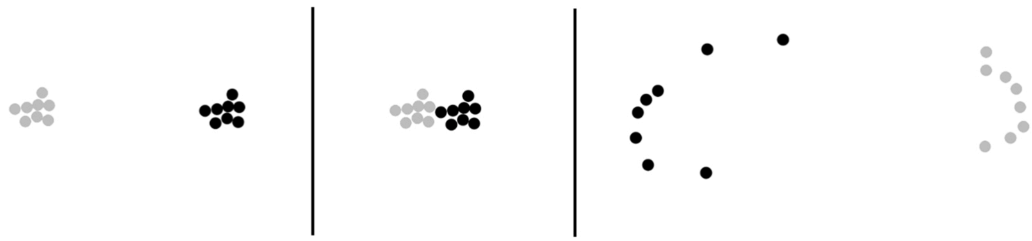

Fig. 20. Schematic collision of XMF agglomerates and subsequent dispersion in the air.

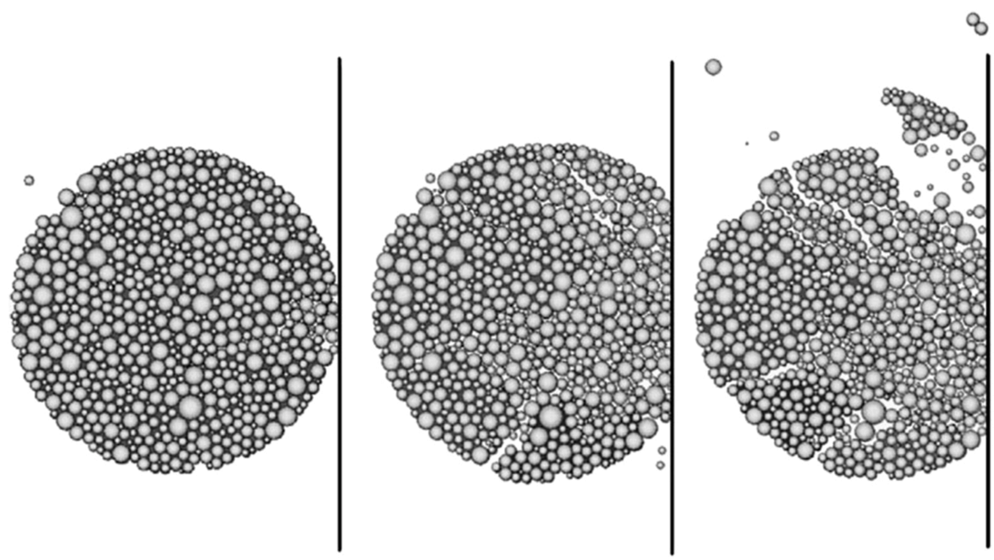

Fig. 21. Fractured specimens of agglomerates collided at different impact velocities according to Antonyuk et al. (2006): left low velocity, middle medium velocity and right high velocity.

fraction particularly interesting regarding workers health and environmental safety.

4. Conclusion

Even though the two bulk materials tested are chemically identical and differ only in their particle size distribution, their behavior with regard to dust emission during discharge of a conveyor belt is fundamentally different. The coarser 0.5–1.2 material primarily emits dust upon impact, whereas the XMF material primarily emits dust during the falling period.

At the tested low wind speeds, the coarser 0.5-1.2 is more susceptible to the surrounding air current. This may seem counterintuitive at first, but it can be explained by comparing the results to modelling approaches from the literature (Schulz et al., 2022).

The finer XMF dust emission is comparatively indifferent to changes in wind speed, within the low speed range tested. Nevertheless, the nature of this fine material gives a much larger potential for dust to potentially be emitted. This can lead to much larger emissions if the wind or other forces are strong enough to disperse the loose agglomerate structure of the XMF during belt discharge.

Comparing the results of the measurement campaign with models in the literature shows that, even though there are good models available to describe individual aspects of dust emission during conveyor belt discharge, there are currently no models that fully describe all aspects of the process.

Understanding the origins of dust can help with handling bulk materials. For 0.5–1.2, this would mean either suppressing the dust release mechanism (fine material being detached from coarse grains) or addressing the main emission location: the impact zone on the bulk material pile. For XMF this would mean to suppress or tread the midair particle-agglomerate to particle-agglomerate interaction.

Further investigations are needed to study possible emission control measures in bulk material discharge from a belt conveyor.

CRediT authorship contribution statement

Marcus Weidemann: Writing – original draft, Visualization, Methodology, Investigation, Formal analysis, Data curation. **Eberhard Schmidt:** Writing – review & editing, Supervision, Project administration, Funding acquisition.

Declaration of competing interest

The authors declare that they have no known competing financial interests or personal relationships that could have appeared to influence the work reported in this paper.

Acknowledgment

The IGF project 21821/N1 of the research association Forschungs-Gesellschaft Verfahrens-Technik e.V. (GVT) was supported in a program to promote the Industrial Community Research and Development (IGF) by the Federal Ministry for Economic Affairs and Energy on the basis of a resolution of the German Bundestag.

References

Ansart, R., de Ryck, A., & Dodds, J. A. (2009). Dust emission in powder handling: Free falling particle plume characterisation. *Chemical Engineering Journal, 152*, 415–420.

Antonyuk, S., Khanal, M., Tomas, J., Heinrich, S., & Mörl, L. (2006). Impact breakage of spherical granules: Experimental study and DEM simulation. *Chemical Engineering and Processing, 45*, 838–856.

Bach, S. (2013). *Beurteilung des Staubungsverhaltens von Pulvern und Schüttgütern - Grenzen und neue Ansätze, Wuppertal*. Shaker Verlag.

Chakravarty, S., Fischer, M., Li Bihan, O., & Morgeneyer, M. (2019). Towards a theoretical understanding of dustiness. *Granular Matter, 21*(97).

Chakravarty, S., Le Bihan, O., Fischer, M., & Morgeneyer, M. (2017). Dust generation in powders: Effect of particle size distribution. In *Powders and grains 2017 – 8th international conference on micromechanics on granular media*. Montpellier.

de Almeida Leão, R. X., Amorim, L. S., Martins, M. F., Junior, H. B., Sarcinelli, E., & Mesquita, A. L. A. (2020). A model for velocity streamlines of airborne dust particles spreading caused by free-falling bulk materials. *Powder Technology, 371*, 190–194.

Derakhshani, S. M. (2016). *Modelling dust liberation in bulk material handling systems*. Delft: Delft University of Technology. Ph.D. Thesis.

Derakhshani, S. M., Schott, D. L., & Lodewijks, G. (2013). Modeling dust liberation at the Belt conveyor transfer point with CFD and DEM. In *11th international Congress on bulk materials storage, handling and transportation*. Newcastle.

Kahrizsangi, H. S., Sofia, D., Barletta, D., & Poletto, M. (2015). Dust generation in vibrated cohesive powders. *Chemical Engineering Transactions, 43*, 769–774.

Londershausen, T. T. (2018). *Entwicklung von Prognosefunktionen zur Abschätzung der Staubungsneigung von trockenen und feuchten Schüttgütern, Aachen*. Shaker Verlag.

Olaleye, B., Pozza, F., Wu, C.-Y., & Liu, L. X. (2019). Population balance modelling of ribbon milling with a new mass-based T breakage function. *International Journal of Pharmaceutics, 571*, Article 118765.

Rheina-Wolbeck, G. (2006). *Entstehung diffuser Staubemissionen während des Fallens von Schüttgütern*. Wien: Dissertation: Technische Universität Wien.

Roberts, J., Andrews, L., & Wypych, P. (2021). Analysis of dust dispersion in the loading of a bulk carrier ship using CFD and DEM. *Particulate Science and Technology, 40*(3), 346–354.

Saleh, K., Jaoude, M.-T. M. A., Morgeneyer, M., Lefrancois, E., Le Bihan, O., & Bouillard, J. (2014). Dust generation from powders: A characterization test based on stirred fluidization. *Powder Technology, 255*, 141–148.

Schmidt, E. (2001). *Kurz gefasste Grundlagen der Partikelcharakterisierung und der Partikelabscheidung*. Shaker: Aachen.

Schulz, D., Schwindt, N., Schmidt, E., Jasevičius, R., & Kruggel-Emden, H. (2019). Investigation of the dust release from bulk material undergoing various mechanical processes using a coupled DEM/CFD approach. *Powder Technology, 355*, 37–56.

Schulz, D., Woschny, N., Schmidt, E., & Kruggel-Emden, H. (2022). Modelling of the detachment of adhesive dust particles during bulk solid particle impact to enhance dust detachment functions. *Powder Technology, 400*.

Teipel, U., Schreiber, A., & Wolf, S. (2023). Einfluss der Partikelgrö ße auf die Staubungsneigung von partikulären Recyclingbaustoffen. *Chemie Ingenieur Technik, 95*(12), 1928–1933.

Turkevich, L. A., Chen, H., & Jog, M. A. (2025). Dust resuspension from the splash of a falling powder: A numerical aerodynamic simulation of a pellet falling onto a powder monolayer. *Aerosol Science and Technology, 59*(1), 49–65.

VDI-Gesellschaft Verfahrenstechnik und Chemieingenieurwesen (GVC). (2013). *VDI-Wärmeatlas* (11th ed.). Düsseldorf: Springer Vieweg.

Weidemann, M., Felder, M., & Schmidt, E. (2023). Development and application of a novel sampling funnel for continuous in-line particle size measurement in dry granulation by roller compaction. In *10th granulation conference*. Sheffield, UK.

Woschny, N. (2025). *Ein Beitrag zur verbesserten Beschreibung der Schüttgutstaubfreisetzung unter Verwendung eines Referenzmaterials, Wuppertal*. Shaker Verlag.

Woschny, N., Schulz, D., Kruggel-Emden, H., & Schmidt, E. (2021). Predicting dust emissions – Experimental study compared to coupled DEM/CFD simulations using a reference test bulk material. *Advanced Powder Technology, 32*, 3189–3206.

Woschny, N., Schulz, D., Kruggel-Emden, H., & Schmidt, E. (2025). A reference material for bulk solid investigations. *Chemical Engineering & Technology, 48*(7), 1–12.

Wypych, P., & Mar, L. (2013). Investigations into the dustiness of bulk materials. *Australian Bulk Handling Review, 18*(1), 64–67.